

Conductance Distribution in Disordered Quantum Wires with a Perfectly Conducting Channel

Yositake TAKANE,¹ Shingo IWASAKI,¹ Yuka YOSHIOKA,¹ Masayuki YAMAMOTO,¹ and Katsunori WAKABAYASHI^{1,2}

¹*Department of Quantum Matter, Graduate School of Advanced Sciences of Matter, Hiroshima University,
Higashihiroshima, Hiroshima 739-8530, Japan*

²*PRESTO, Japan Science and Technology Agency (JST), Kawaguchi, Saitama 332-0012, Japan*

(Received

)

We study the conductance of phase-coherent disordered quantum wires focusing on the case in which the number of conducting channels is imbalanced between two propagating directions. If the number of channels in one direction is by one greater than that in the opposite direction, one perfectly conducting channel without backscattering is stabilized regardless of wire length. Consequently, the dimensionless conductance does not vanish but converges to unity in the long-wire limit, indicating the absence of Anderson localization. To observe the influence of a perfectly conducting channel, we numerically obtain the distribution of conductance in both cases with and without a perfectly conducting channel. We show that the characteristic form of the distribution is notably modified in the presence of a perfectly conducting channel.

KEYWORDS: perfectly conducting channel, DMPK equation, graphene nanoribbon, unitary class

1. Introduction

The discovery of a perfectly conducting channel in disordered carbon nanotubes^{1–4} and graphene nanoribbons^{5,6} provides a counterexample to the conjecture that an ordinary quasi-one-dimensional quantum system with disorder exhibits Anderson localization. The band structure of carbon nanotubes and graphene nanoribbons has two energy valleys near the Dirac points, which are well separated in momentum space. Ando and co-workers have shown that a perfectly conducting channel without backscattering appears in each valley of a metallic carbon nanotube when impurity scattering does not connect the two valleys.^{1–4} Such a situation can be realized when only long-ranged impurities are distributed. The presence of a perfectly conducting channel is concluded from the facts that the reflection matrix r for each valley has the skew-symmetry (i.e., ${}^t r = -r$) and that the number of conducting channels is odd in each valley. It has been pointed out that a perfectly conducting channel is not intrinsic to carbon nanotubes with long-ranged disorder, but universally appears in disordered quasi-one-dimensional systems which belong to the symplectic universality class with an odd number of conducting channels.^{7–16} Note that the symplectic universality class consists of systems having time-reversal symmetry without spin-rotation invariance. The discovery of a perfectly conducting channel in the symplectic universality class resolves the long-standing puzzle raised by Zirnbauer and co-workers.^{17–19} The presence of a perfectly conducting channel in graphene nanoribbons with two zigzag edges has been pointed out by Wakabayashi and co-workers.^{5,6} As in the case of carbon nanotubes, its presence is ensured only when impurities are long-ranged. However, the corresponding stabilization mechanism of a perfectly conducting channel is completely different from that in the case of carbon nanotubes. In each valley of a graphene nanoribbon with two zigzag edges, the number of conducting channels in one propagating

direction is by one greater, or smaller, than that in the opposite direction because each valley has an excess one-way channel. This imbalance results in the appearance of a perfectly conducting channel.^{20,21} The presence of a perfectly conducting channel is a universal characteristic emerging in disordered quasi-one-dimensional systems which belong to the unitary universality class with the channel-number imbalance between two propagating directions.^{16,20–26} The unitary universality class is characterized by the absence of time-reversal symmetry.

The behavior of the dimensionless conductance in such systems with a perfectly conducting channel has been studied by means of the scaling theory based on a random-matrix model,^{7,8,11,13,23,25,26} the super-symmetric field theory,^{9,13} the mapping to a super-spin chain model,^{24,25} and numerical simulations.^{10,12,14–16,20–22} It has been shown that the dimensionless conductance decays exponentially with increasing system length L towards unity, indicating the absence of Anderson localization. This behavior should be contrasted to that in the ordinary case without a perfectly conducting channel, in which the dimensionless conductance vanishes in the long- L limit. It has also been shown that the dimensionless conductance in the presence of a perfectly conducting channel decays much faster than that in the ordinary case. To deeply understand such peculiar transport properties of the systems with a perfectly conducting channel, it is desirable to study the distribution of dimensionless conductance.

For simplicity, we hereafter restrict our attention to disordered quantum wires with unitary symmetry. We consider wires of length L with N right-moving channels and $N + m$ left-moving channels with $m = 0, 1$. In the ordinary case of $m = 0$, the right-moving channels and the left-moving channels have the same set of transmission eigenvalues $\{T_1, T_2, \dots, T_N\}$. Therefore, the dimensionless conductance G_L and G_R for the left-moving and right-moving channels, respectively, are equivalent and

are given by $G_R = G_L = g$ with $g = \sum_{a=1}^N T_a$. In the case of $m = 1$, one left-moving channel becomes perfectly conducting and G_L and G_R differ from each other. If the set of transmission eigenvalues for the right-moving channels is $\{T_1, T_2, \dots, T_N\}$, that for the left-moving channels is expressed as $\{T_1, T_2, \dots, T_N, 1\}$, where we have identified the $N+1$ th channel as the perfectly conducting one.²³ We obtain $G_L = g + 1$ and $G_R = g$ with $g = \sum_{a=1}^N T_a$. The above argument indicates that in both the cases of $m = 0$ and of $m = 1$, we can completely describe the statistical property of G_L and G_R if the distribution of g is given as a function of the wire length L . Let $p(g)$ be the distribution of g . As the averaged conductance $\langle g \rangle$ monotonically decreases with increasing L , we employ it as the scaling parameter instead of L . In the absence of a perfectly conducting channel (i.e., $m = 0$), it has been shown that the characteristic form of $p(g)$ crucially depends on $\langle g \rangle$; the dimensionless conductance g obeys a Gaussian distribution in the short-wire regime of $\langle g \rangle \gg 1$,²⁷ while a log-normal distribution is expected in the long-wire regime of $\langle g \rangle \ll 1$.²⁸ It has also been shown that an interesting behavior appears in the crossover regime of $\langle g \rangle \sim 1$.^{29,30} It is interesting how the behavior of $p(g)$ is affected by the presence of a perfectly conducting channel.

In this paper, we theoretically study the behavior of $p(g)$ in disordered quantum wires with unitary symmetry focusing on the crossover regime of $\langle g \rangle \sim 1$. We obtain $p(g)$ in both the cases of $m = 0$ and of $m = 1$ at $\langle g \rangle = 1.0, 0.5$ and 0.35 . To obtain $p(g)$, we first adopt a classical Monte Carlo approach based on the existing scaling theory. Employing an approximate analytic expression of the probability distribution function of transmission eigenvalues, we calculate $p(g)$ by using a classical Monte Carlo method. For comparison, we also calculate $p(g)$ by adopting a numerical simulation approach with a tight-binding model. For the case of $m = 0$, we employ the tight-binding model for a graphene nanoribbon with zigzag and bearded edges, while the tight-binding model for a graphene nanoribbon with two zigzag edges is employed for the case of $m = 1$. We confirm that the Monte Carlo approach and the numerical simulation approach provide qualitatively identical results. We show that at $\langle g \rangle = 1.0$ (i.e., near the diffusive regime), the distribution $p(g)$ in the case of $m = 1$ is similar to that in the ordinary case of $m = 0$. However, a notable difference appears for the smaller values of $\langle g \rangle$. It is shown that in the case of $m = 0$, the distribution $p(g)$ at both $\langle g \rangle = 0.5$ and 0.35 are cut off when g exceeds unity, resulting in the appearance of a kink near $g = 1$,^{29,30} while no such structure appears in the case of $m = 1$. This indicates that the absence of a kink in $p(g)$ is a notable characteristic of disordered quantum wires with a perfectly conducting channel. We explain this behavior from the viewpoint of eigenvalue repulsion due to the perfectly conducting transmission eigenvalue.

In the next section, we obtain the conductance distribution $p(g)$ by using a classical Monte Carlo approach based on the scaling theory. In §3, we obtain $p(g)$ by using a numerical simulation approach with a tight-binding model. Section 4 is devoted to summary.

2. Monte Carlo Approach

We present the scaling theory based on a random-matrix model to describe electron transport properties in systems with the channel-number imbalance.²³ Let us consider disordered wires with N right-moving channels and $N + m$ left-moving channels with $m = 0, 1$. As discussed in the previous section, the dimensionless conductance G_L and G_R are expressed in terms of $g \equiv \sum_{a=1}^N T_a$ as $G_L = m + g$ and $G_R = g$. It should be noted that the mean free paths l and l' for the left-moving and right-moving channels, respectively, are not equal if $m \neq 0$. Indeed, they satisfy $l' = (N/(N + m))l$. The statistical behavior of g is described by the probability distribution of $\{T_1, T_2, \dots, T_N\}$. We define $\lambda_a \equiv (1 - T_a)/T_a$ and introduce the probability distribution $P(\{\lambda_a\}; s)$ of $\{\lambda_1, \lambda_2, \dots, \lambda_N\}$, where s is the normalized system length defined by $s \equiv L/l$. The Fokker-Planck equation for $P(\{\lambda_a\}; s)$, which is called the Dorokhov-Mello-Pereyra-Kumar (DMPK) equation,^{31,32} is expressed as²³

$$\frac{\partial P(\{\lambda_a\}; s)}{\partial s} = \frac{1}{N} \sum_{a=1}^N \frac{\partial}{\partial \lambda_a} \left(\lambda_a (1 + \lambda_a) J \frac{\partial}{\partial \lambda_a} \left(\frac{P(\{\lambda_a\}; s)}{J} \right) \right) \quad (1)$$

with

$$J = \prod_{c=1}^N \lambda_c^m \times \prod_{b=1}^{N-1} \prod_{a=b+1}^N |\lambda_a - \lambda_b|^2. \quad (2)$$

The factor $\prod_{c=1}^N \lambda_c^m$ in J represents the repulsion arising from the perfectly conducting eigenvalue. This eigenvalue repulsion suppresses non-perfectly conducting eigenvalues $\{T_1, T_2, \dots, T_N\}$. It should be emphasized that the influence of a perfectly conducting channel is described by only this factor.

We numerically calculate $p(g)$ by using a classical Monte Carlo approach based on an approximate probability distribution of transmission eigenvalues. The probability distribution can be obtained from the exact solution of the DMPK equation.^{33,34} We define x_a by the relation of $\lambda_a \equiv \sinh^2 x_a$. In terms of a set of variables $\{x_a\}$, the probability distribution is given by²⁶

$$P(\{x_a\}; s) = \text{const.} \cdot e^{-H(\{x_a\})} \quad (3)$$

with

$$H(\{x_a\}) = \sum_{a=1}^N \left(\frac{N}{s} x_a^2 - \left(m + \frac{1}{2} \right) \ln |x_a \sinh 2x_a| \right) - \sum_{a,b=1(a>b)}^N \left(\ln |\sinh^2 x_a - \sinh^2 x_b| + \ln |x_a^2 - x_b^2| \right). \quad (4)$$

Although eq. (3) is derived under the assumption of $s/4N \ll 1$, we can expect that it is qualitatively reliable even when $s/4N \sim 1$.²⁶ Note that g is expressed as $g = \sum_{a=1}^N 1/\cosh^2 x_a$.

We can interpret $H(\{x_a\})$ as the Hamiltonian function of N classical particles in one dimension. This analogy

allows us to adapt a Monte Carlo approach to numerical calculations of $p(g)$. Using a simple Metropolis algorithm,^{30,35} we obtain $p(g)$ for $N = 5$ in both the cases of $m = 0$ and of $m = 1$ at $\langle g \rangle = 1.0, 0.5$ and 0.35 . By numerically calculating $\langle g \rangle$ as a function of the normalized system length s , we find that $\langle g \rangle = 1.0$ at $s/N = 0.77$ (0.45), $\langle g \rangle = 0.5$ at $s/N = 1.59$ (0.75) and $\langle g \rangle = 0.35$ at $s/N = 2.15$ (0.91) for $m = 0$ ($m = 1$). As pointed out in ref 23, the decrease of $\langle g \rangle$ as a function of s becomes fast with increasing m due to the eigenvalue repulsion arising from the perfectly conducting eigenvalue $T = 1$. Therefore, the value of s/N yielding a given $\langle g \rangle$ for $m = 1$ is smaller than that for $m = 0$.

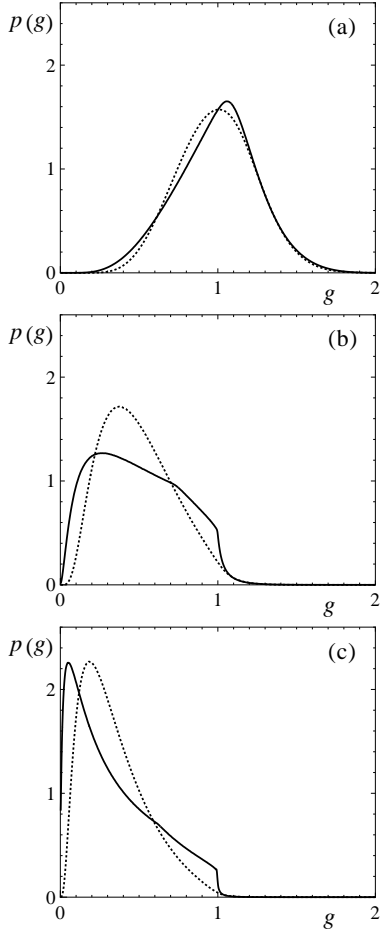


Fig. 1. The conductance distributions at (a) $\langle g \rangle = 1.0$, (b) $\langle g \rangle = 0.5$ and (c) $\langle g \rangle = 0.35$ for $m = 0$ (solid lines) and $m = 1$ (dotted lines).

The resulting conductance distributions are shown in Fig. 1. Each distribution is obtained by using 2×10^9 Monte Carlo steps. Except for the case of $\langle g \rangle = 1.0$, a notable difference appears between the result for $m = 0$ and that for $m = 1$. In the ordinary case of $m = 0$, the distributions at both $\langle g \rangle = 0.5$ and 0.35 are cut off when g exceeds unity, resulting in the appearance of a kink near $g = 1$.^{29,30} We observe that no such structure appears when $m = 1$. The behavior similar to this has been observed in the numerical result of refs. 16 and 22.

We explain this behavior as follows. In the crossover

regime, g is dominated by the largest transmission eigenvalue T_1 and the second-largest one T_2 . That is, $g \approx T_1 + T_2$. In the case of $m = 0$, the largest eigenvalue T_1 can become nearly equal to unity. However, the second-largest eigenvalue T_2 is suppressed by the eigenvalue repulsion from T_1 and thus $T_2 \ll T_1 \leq 1$. Therefore, g rarely becomes larger than unity, resulting in the appearance of the kink near $g = 1$. In contrast, T_1 in the case of $m = 1$ cannot become nearly equal to unity due to the eigenvalue repulsion from the perfectly conducting eigenvalue. Therefore, $p(g)$ near $g = 1$ is suppressed and the kink disappears. We also observe that in the case of $m = 1$, the distribution is suppressed near $g = 0$, as well as $g = 1$, and the width of $p(g)$ becomes narrow. The suppression near $g = 0$ simply reflects the fact that s/N yielding a given $\langle g \rangle$ is smaller in the case of $m = 1$ than in the case of $m = 0$. From eq. (4), we understand that smaller s/N results in smaller $\{x_a\}$ and therefore g tends to become large. Thus, $p(g)$ near $g = 0$ is more suppressed in the case of $m = 1$ than in the case of $m = 0$.

We finally note that in the case of $m = 0$ without a perfectly conducting channel, $p(g)$ at $\langle g \rangle = 0.5$ is similar to the critical conductance distribution for the quantum Hall transition³⁶ and $p(g)$ at $\langle g \rangle = 0.35$ is similar to the critical conductance distribution for the Anderson transition in three dimensions.³⁷

3. Numerical Simulation Approach

In this section, we calculate conductance distributions by adopting a numerical simulation approach. As model systems, we consider a graphene nanoribbon with zigzag and bearded edges (zigzag-bearded nanoribbon) and a graphene nanoribbon with two zigzag edges (zigzag-zigzag nanoribbon) (see Fig. 2). In the following, we fix

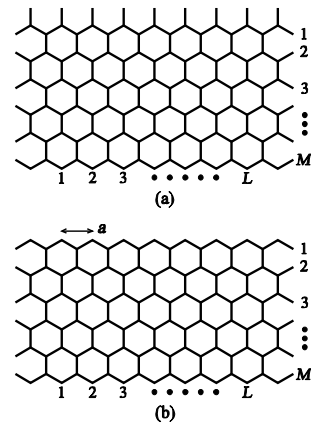


Fig. 2. The structures of (a) zigzag-bearded nanoribbon and (b) zigzag-zigzag nanoribbon.

the number of lattice sites in the transverse direction to be $M = 30$. We describe electronic states of these nanoribbons by using a tight-binding model on the honeycomb lattice. For the case of $m = 0$, we employ the tight-binding model for the zigzag-bearded nanoribbon, while that for the zigzag-zigzag nanoribbon is employed

for the case of $m = 1$. The tight-binding model is given by

$$H = - \sum_{i,j} \gamma_{i,j} |i\rangle \langle j| + \sum_i V_i |i\rangle \langle i|, \quad (5)$$

where $|i\rangle$ and V_i represent the localized electron state and the impurity potential, respectively, on site i , and $\gamma_{i,j}$ is the transfer integral between sites i and j . We assume that $\gamma_{i,j} = t$ if i and j are nearest neighbors and $\gamma_{i,j} = 0$ otherwise. The band structures obtained from this tight-binding model without disorder are displayed in Fig. 3. We observe that the zigzag-bearded nanoribbon has a completely flat band,^{6,38} while a partially flat band appears in the zigzag-zigzag nanoribbon,³⁹ and that both of them commonly possess two energy valleys. The right and left valleys are referred to as K_+ and K_- valleys, respectively. We assume that impurity potential arising from each scatterer has a spatial range greater than the lattice constant a . In this case, inter-valley scattering is not induced by such long-ranged impurity potential, and the two energy valleys are disconnected. Thus, these energy valleys independently contribute electron transport. Hereafter, we restrict our consideration to the case in which the Fermi energy E is placed within $0 < E/t < 1$. Note that in the zigzag-zigzag nanoribbon, the partially flat band provides an excess left-moving (right-moving) channel in the K_+ (K_-) valley. Therefore, the number N_L of left-moving channels is by one greater (smaller) than the number N_R of right-moving channels in the K_+ (K_-) valley. That is, $N_L = N_R + 1$ in the K_+ valley and

$N_L + 1 = N_R$ in the K_- valley. This results in the appearance of one perfectly conducting channel in both the left-moving channels in the K_+ valley and the right-moving channels in the K_- valley.^{5,6} In contrast, N_L and N_R are equal to each other in both the valleys of the zigzag-bearded nanoribbon and no perfectly conducting channel appears. Let G_L^\pm and G_R^\pm be the dimensionless conductance for the left-moving channels and that for the right-moving channels in the valley K_\pm . For the case of the zigzag-bearded nanoribbon with $N_L = N_R = N$ in both the valleys, we observe that $G_L^+ = G_R^+ = G_L^- = G_R^- = g$ with $g = \sum_{a=1}^N T_a$. In contrast, for the case of the zigzag-zigzag nanoribbon with $N_L - 1 = N_R = N$ in the K_+ valley and $N_L = N_R - 1 = N$ in the K_- valley (see Table I), we observe that $G_R^+ = G_L^- = g$ and $G_L^+ = G_R^- = 1 + g$ with $g = \sum_{a=1}^N T_a$. Note that G_L^+ and G_R^- contains the contribution from one perfectly conducting channel. The total conductance of these systems is expressed as $G_{\text{total}} = m + 2g$ with $m = 0$ for the zigzag-bearded nanoribbon and $m = 1$ for the zigzag-zigzag nanoribbon.

Table I. The number of left-moving channels, N_L , and the number of right-moving channels, N_R , where $m = 0$ for the zigzag-bearded nanoribbon and $m = 1$ for the zigzag-zigzag nanoribbon.

| Valley | N_L | N_R |
|--------|---------|---------|
| K_+ | $N + m$ | N |
| K_- | N | $N + m$ |

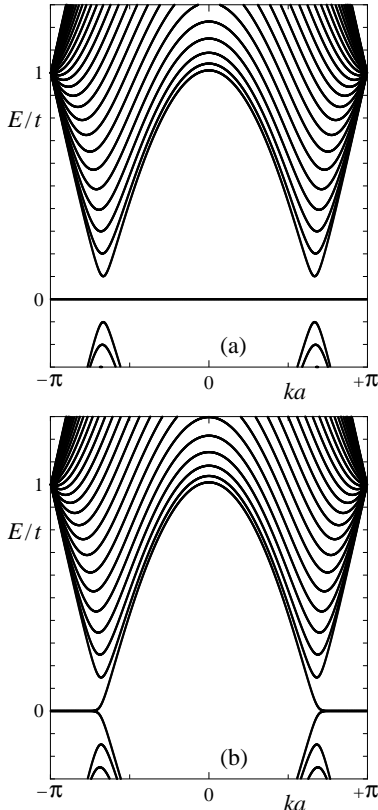


Fig. 3. The band structures of (a) zigzag-bearded nanoribbon and (b) zigzag-zigzag nanoribbon with $M = 30$.

Let us consider nanoribbons which is infinitely long in the longitudinal direction. To introduce disorder, we randomly distribute scatterers in the finite region of L lattice sites. We identify L with the length of our system. We assume that the impurity potential on site i arising from a scatterer at site j is given by

$$V_i(j) = w_j \exp(-|\mathbf{r}_i - \mathbf{r}_j|^2/d^2), \quad (6)$$

where \mathbf{r}_i is the position vector of site i , and w_j and d represent the amplitude and the spatial range of this potential, respectively. Thus, the impurity potential on site i is given by

$$V_i = \sum_j V_i(j), \quad (7)$$

where j is summed over the disordered region of length L . The amplitude w_j is distributed uniformly within the range of $-W/2 < w_j < W/2$. Let p be the probability that each site is occupied by a scatterer. The strength of disorder is controlled by W and p . Adopting the model described above, we calculate the dimensionless conductance G_{total} by using the Landauer formula

$$G_{\text{total}} = \text{tr}\{\mathbf{t}\mathbf{t}^\dagger\}, \quad (8)$$

where \mathbf{t} is the transmission matrix through the disordered region. The dimensions of \mathbf{t} are equal to $(2N+m) \times (2N+m)$. We consider the behavior of $g \equiv (G_{\text{total}} - m)/2$ in the case of $N = 5$. With $M = 30$, this is realized when $0.486 \leq E/t \leq 0.571$ for the zigzag-bearded nanoribbon

($m = 0$) and $0.529 \leq E/t \leq 0.611$ for the zigzag-zigzag nanoribbon ($m = 1$). The following parameters are employed: $W/t = 0.1$, $p = 0.1$ and $d/a = 1.5$ with a being the lattice constant (see Fig 2(b)). We can numerically obtain \mathbf{t} for a given impurity configuration by using a recursive Green's function technique.

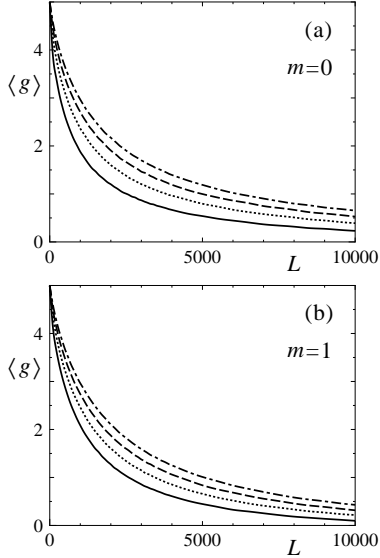


Fig. 4. The average of g for $N = 5$ with (a) $m = 0$ and (b) $m = 1$ as a function of the length L , where $E/t = 0.49, 0.50, 0.51$ and 0.52 from bottom to top in the case of $m = 0$ and $E/t = 0.54, 0.55, 0.56$ and 0.57 from bottom to top in the case of $m = 1$.

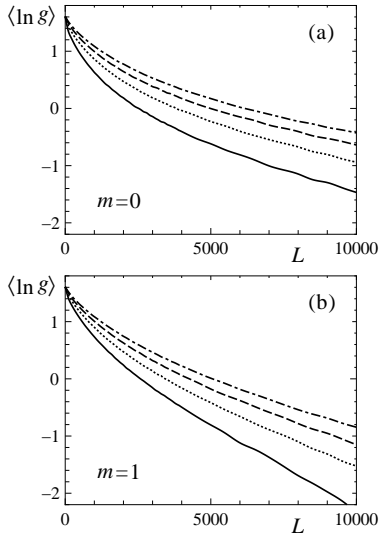


Fig. 5. The average of $\ln g$ for $N = 5$ with (a) $m = 0$ and (b) $m = 1$ as a function of the length L , where $E/t = 0.49, 0.50, 0.51$ and 0.52 from bottom to top in the case of $m = 0$ and $E/t = 0.54, 0.55, 0.56$ and 0.57 from bottom to top in the case of $m = 1$.

Before studying the conductance distribution, we consider the behavior of the ensemble averages of g and $\ln g$.

We numerically calculate $\langle g \rangle$ and $\langle \ln g \rangle$ as a function of L at $E/t = 0.49, 0.50, 0.51$ and 0.52 for the case of $m = 0$ and at $E/t = 0.54, 0.55, 0.56$ and 0.57 for the case of $m = 1$. Figures 4 and 5 show the L -dependence of $\langle g \rangle$ and $\langle \ln g \rangle$, respectively. The ensemble average for each data point is performed over 5000 samples with different impurity configuration. We observe from Fig. 4 that the decay of $\langle g \rangle$ with increasing L becomes slower with increasing E/t in both the cases of $m = 0$ and of $m = 1$. This implies that the mean free path l becomes longer with increasing E/t . Although the decay of $\langle g \rangle$ seems to be slightly faster in the case of $m = 1$ than in the ordinary case of $m = 0$, we cannot state this definitively. However, Fig. 5 clearly shows that $\langle \ln g \rangle$ decreases faster in the case of $m = 1$ than in the case of $m = 0$. This is consistent with the scaling theory²³ and is explained as follows. In the case of $m = 1$, one perfectly conducting channel is present and the corresponding transmission eigenvalue (i.e., $T = 1$) suppresses the other transmission eigenvalues $\{T_1, T_2, \dots, T_N\}$ due to eigenvalue repulsion. This results in the suppression of g . Indeed, the scaling theory predicts that the conductance decay length ξ defined by $\exp[\langle \ln g \rangle] \equiv \exp[-2L/\xi]$ is given by²³

$$\xi = \frac{2Nl}{m+1}, \quad (9)$$

indicating that ξ in the case of $m = 1$ is twice shorter than that in the case of $m = 0$ if the mean free path is common to the two cases. We estimate ξ from the result of $\langle \ln g \rangle$. The estimated values of ξ are listed in Table II. Because the mean free path should depend on E/t and m , a detailed comparison with eq. (9) is not straightforward. However, we observe the obvious tendency that ξ in the case of $m = 1$ is shorter than that in the case of $m = 0$. This is consistent with the prediction of the scaling theory.

Table II. The conductance decay length ξ in the cases of $m = 0$ and of $m = 1$ for several values of E/t .

| $m = 0$ | | $m = 1$ | |
|---------|-------|---------|-------|
| E/t | ξ | E/t | ξ |
| 0.49 | 11500 | 0.54 | 6400 |
| 0.50 | 13500 | 0.55 | 8400 |
| 0.51 | 15100 | 0.56 | 9500 |
| 0.52 | 15900 | 0.57 | 10600 |

Now, we consider the conductance distribution $p(g)$. We numerically obtain $p(g)$ at $\langle g \rangle = 1.0, 0.5$ and 0.35 in both the cases of $m = 0$ and of $m = 1$. We set $E/t = 0.49$ for $m = 0$ and $E/t = 0.54$ for $m = 1$. From the numerical result displayed in Fig. 4, we find that $\langle g \rangle = 1.0$ at $L = 2511$ (2583), $\langle g \rangle = 0.5$ at $L = 5352$ (4623) and $\langle g \rangle = 0.35$ at $L = 7312$ (5801) for $m = 0$ ($m = 1$). The resulting conductance distributions for the case of $m = 0$ and those for the case of $m = 1$ are displayed in Figs. 6 and 7, respectively, where each distribution is obtained by using 5×10^5 samples. For comparison, we also display the conductance distributions obtained by the Monte Carlo approach. We observe that the result of the numerical

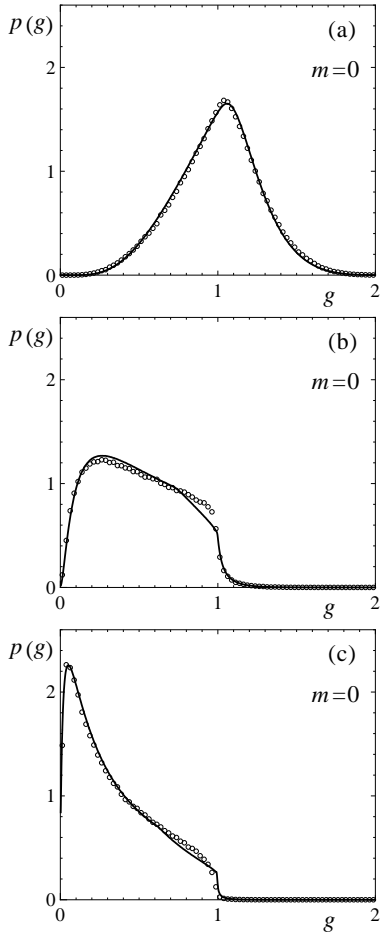


Fig. 6. The conductance distributions for the case of $m = 0$ at (a) $\langle g \rangle = 1.0$, (b) $\langle g \rangle = 0.5$ and (c) $\langle g \rangle = 0.35$. Open circles represent the numerical simulation result, while solid lines represent the Monte Carlo result.

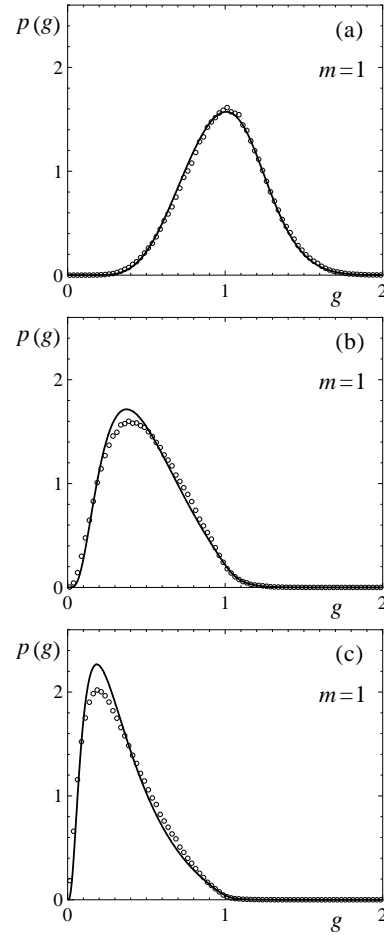


Fig. 7. The conductance distributions for the case of $m = 1$ at (a) $\langle g \rangle = 1.0$, (b) $\langle g \rangle = 0.5$ and (c) $\langle g \rangle = 0.35$. Open circles represent the numerical simulation result, while solid lines represent the Monte Carlo result.

simulation approach is qualitatively identical to that of the Monte Carlo approach for both the cases of $m = 0$ and of $m = 1$. Particularly, we again observe a kink near $g = 1$ in the case of $m = 0$ at $\langle g \rangle = 0.5$ and 0.35 , while no such structure appears in the case of $m = 1$.

We finally note that a relatively large deviation between the two results appears in the case of $m = 1$ for $\langle g \rangle = 0.5$ and 0.35 , while no such deviation is observed in the case of $m = 0$. This reflects the fact that the probability distribution $P(\{x_a\}; s)$ given in eq. (3) overestimates the influence of a perfectly conducting channel in the long-wire regime of $s/N \gtrsim 1^{26}$ although this is a very good approximation irrespective to s/N in the case of $m = 0$ without a perfectly conducting channel.³⁰

4. Summary

The dimensionless conductance g in disordered quantum wires with unitary symmetry is studied for both cases with and without a perfectly conducting channel. To observe the influence of a perfectly conducting channel on the behavior of g , we have calculated the conductance distribution $p(g)$ for these two cases in the crossover regime where $\langle g \rangle$ is slightly smaller than unity. We have adopted two approaches, a classical Monte Carlo approach based on the existing scaling theory and a nu-

merical simulation approach with a tight-binding model. In the latter approach, we have employed the tight-binding model for a graphene nanoribbon with two zigzag edges (zigzag and bearded edges) for the case with (without) a perfectly conducting channel. We have confirmed that the two approaches provide qualitatively identical results. It is shown that in the absence of a perfectly conducting channel, the distribution $p(g)$ are cut off when g exceeds unity, resulting in the appearance of a kink near $g = 1$, while no such structure appears in the presence of a perfectly conducting channel. This indicates that the absence of a kink in $p(g)$ is a notable characteristic of disordered quantum wires with a perfectly conducting channel.

Acknowledgment

K. W. acknowledges the financial support by a Grant-in-Aid for Young Scientists (B) (No. 19710082) and Specially Promoted Research (No. 20001006) from the Ministry of Education, Culture, Sports, Science and Technology, also by a Grand-in-Aid for Scientific Research (B) from the Japan Society for the Promotion of Science (No. 19310094).

- 1) T. Ando and T. Nakanishi: J. Phys. Soc. Jpn. **67** (1998) 1704.
- 2) T. Ando, T. Nakanishi, and R. Saito: J. Phys. Soc. Jpn. **67** (1998) 2857.
- 3) T. Nakanishi and T. Ando: J. Phys. Soc. Jpn. **68** (1999) 561.
- 4) T. Ando and H. Suzuura: J. Phys. Soc. Jpn. **71** (2002) 2753.
- 5) K. Wakabayashi, Y. Takane, and M. Sigrist: Phys. Rev. Lett. **99** (2007) 036601.
- 6) K. Wakabayashi, Y. Takane, M. Yamamoto, and M. Sigrist: Carbon **47** (2009) 124.
- 7) Y. Takane and K. Wakabayashi: J. Phys. Soc. Jpn. **72** (2003) 2710.
- 8) Y. Takane: J. Phys. Soc. Jpn. **73** (2004) 9.
- 9) Y. Takane: J. Phys. Soc. Jpn. **73** (2004) 1430.
- 10) Y. Takane: J. Phys. Soc. Jpn. **73** (2004) 2366.
- 11) H. Sakai and Y. Takane: J. Phys. Soc. Jpn. **74** (2005) 1521.
- 12) T. Ando: J. Phys. Soc. Jpn. **75** (2006) 054701.
- 13) H. Sakai and Y. Takane: J. Phys. Soc. Jpn. **75** (2006) 054711.
- 14) H. Sakai, K. Wakabayashi, and Y. Takane: J. Phys. Soc. Jpn. **76** (2007) 034717.
- 15) H. Obuse, A. Furusaki, S. Ryu, and C. Mudry: Phys. Rev. B **78** (2008) 115301.
- 16) K. Kobayashi, K. Hirose, H. Obuse, T. Ohtsuki, and K. Slevin: arXiv:0809.1146.
- 17) On the basis of a supersymmetric field theory, Zirnbauer and co-workers^{18,19} claimed that the averaged dimensionless conductance $\langle g \rangle$ in the symplectic universality class converges to $1/2$ in the long-wire limit and thus Anderson localization is absent. At present, we understand that the averaged conductance they obtained is nothing but the arithmetic average of $\langle g_{\text{even}} \rangle$ for the even-channel case and $\langle g_{\text{odd}} \rangle$ for the odd-channel case. See the discussion given in refs. 9 and 13. References 18 and 19 should be regarded as the first report that suggests a possibility of delocalization in disordered wires with symplectic symmetry. However, they recognized neither the even-odd difference nor the presence of a perfectly conducting channel.
- 18) M. R. Zirnbauer: Phys. Rev. Lett. **69** (1992) 1584.
- 19) A. D. Mirlin, A. Müller-Groeling, and M. R. Zirnbauer: Ann. Phys. (New York) **236** (1994) 325.
- 20) C. Barnes, B. L. Johnson, and G. Kirczenow: Phys. Rev. Lett. **70** (1993) 1159.
- 21) C. Barnes, B. L. Johnson, and G. Kirczenow: Can. J. Phys. **72** (1994) 559.
- 22) K. Hirose, T. Ohtsuki, and K. Slevin: Physica E **40** (2008) 1677.
- 23) Y. Takane and K. Wakabayashi: J. Phys. Soc. Jpn. **76** (2007) 053701.
- 24) Y. Takane and K. Wakabayashi: J. Phys. Soc. Jpn. **76** (2007) 083710.
- 25) Y. Takane: J. Phys. Soc. Jpn. **77** (2008) 014703.
- 26) Y. Takane and K. Wakabayashi: J. Phys. Soc. Jpn. **77** (2008) 054702.
- 27) V. A. Gopar, M. Martínez, and P. A. Mello: Phys. Rev. B **51** (1995) 16917.
- 28) J.-L. Pichard: in *Quantum Coherence in mesoscopic Systems*, ed. B. Kramer (Plenum Press, New York, 1991) p. 369.
- 29) K. A. Muttalib and P. Wölfe: Phys. Rev. Lett. **83** (1999) 3013.
- 30) L. S. Froufe-Pérez, P. García-Mochales, P. A. Serena, P. A. Mello, and J. J. Sáenz: Phys. Rev. Lett. **89** (2002) 246403.
- 31) O. N. Dorokhov: JETP. Lett. **36** (1982) 318.
- 32) P. A. Mello, P. Pereyra, and N. Kumar: Ann. Phys. (New York) **181** (1988) 290.
- 33) C. W. J. Beenakker and B. Rejaei: Phys. Rev. B **49** (1994) 7499.
- 34) T. Akuzawa and M. Wadati: J. Phys. A **31** (1998) 1713.
- 35) C. M. Canali: Phys. Rev. B **53** (1996) 3713.
- 36) T. Ohtsuki, K. Slevin, and B. Kramer: Physica E **22** (2004) 248.
- 37) K. Slevin and T. Ohtsuki: Phys. Rev. Lett. **78** (1997) 4083.
- 38) K. Wakabayashi: Thesis, University of Tsukuba (2000) [<http://hdl.handle.net/2241/2592>].
- 39) M. Fujita, K. Wakabayashi, K. Nakada, and K. Kusakabe: J. Phys. Soc. Jpn. **65** (1996) 1920.